



ARTICLE

# The Spatial and Electronic Effects of Substituent Groups on the Thermal Curing of Bio-Based Benzoxazines

Rumeng Li<sup>1</sup>, Guozhu Zhan<sup>2</sup>, Qi Ma<sup>1</sup>, Yunhe Yang<sup>1</sup>, Xiaoyun Liu<sup>1,\*</sup>, Yitong Zhang<sup>1</sup> and Qixin Zhuang<sup>1</sup>

<sup>1</sup>Laboratory of Specially Functional Polymeric Materials and Related Technology (ECUST), Ministry of Education, East China University of Science and Technology, Shanghai, 200237, China

<sup>2</sup>The 806th Institute of the Eighth Academy of CASC, Huzhou, 313000, China

\*Corresponding Author: Xiaoyun Liu. Email: liuxiaoyun@ecust.edu.cn

Received: 17 January 2021 Accepted: 05 March 2021

## ABSTRACT

To explore the influence of substituent groups on thermally induced curing, eight new bio-based benzoxazines containing different substituent groups with different electron negativity and volumes were synthesized. The thermal curing of these bio-based benzoxazines was studied in detail. Combined with the curing reaction kinetics, simulation and calculation of Highest Occupied Molecular and Lowest Unoccupied Molecular values, the spatial and electronic effects of different substituent groups on the curing of benzoxazine was explored. It was found that when the substituent was located at the position directly connected to the N atom, the steric hindrance effect of the group was dominant. When the substituent group was located on the benzene ring connected to the O atom, both the electronic effect and the spatial effect influenced the curing of benzoxazine. When an electron-withdrawing group was connected ortho position to the O atom, the curing reaction was promoted due to the decreased electron cloud density of O<sup>-</sup> on the oxazine ring, making the C-O bond easier to break. When an electron-donating group was connected to the meta position of the O atom it also promoted the curing reaction, possibly because it increased the electron cloud density of the <sup>+</sup>CH<sub>2</sub> reaction site and thereby facilitated electrophilic substitution via attack of <sup>+</sup>CH<sub>2</sub> on the cross linking reaction centre. This work provides a deeper understanding of how spatial and electronic effects of substituents affect the curing of benzoxazine.

## KEYWORDS

Benzoxazine; spatial effects; electronic effects; bio-based

## 1 Introduction

As a new type of phenolic resin, polybenzoxazine (PBz) resin has overcome many disadvantages of traditional phenolic resins and aroused extensive research interest. In contrast to traditional thermosetting resins, benzoxazine resin has almost no volume shrinkage in the process of heat curing [1]. This is beneficial in the preparation of fibre-reinforced composite materials. The structure of PBz is compact, which minimizes the formation of pore defects in the preparation process and greatly enhances the bonding strength between the fibre and the resin in the composite material. In addition, due to a large number of hydroxyl and tertiary amine groups inside the molecule—which generate a large number of intra- and inter-molecular hydrogen bonds [2–7]—PBz also has advantages such as a high glass transition



temperature, low moisture absorption, high char yield, excellent dielectric properties, tensile strength and modulus, flame retardancy with low smoke and toxicity, and low surface energy [8–11]. Additionally, the benzoxazine structure can be designed flexibly according to the demands of the application, with functional groups such as allyl, propargyl, diacetylene, nitrile, furyl, epoxide, amino and siloxy groups able to be introduced into its molecular structure [12–26]. Because of its excellent thermal and mechanical properties, PBz resins have gradually become an alternative to traditional phenolic, epoxy, bismaleimide and other thermosetting resins in practical applications including high-temperature resistant materials [27–33], flame retardant materials [34–37], electronic packaging materials [38] and composite matrixes [39–42].

However, benzoxazine has the disadvantage of a high curing temperature [43–45]. An understanding of how the molecular chemical structure of benzoxazine influences its thermal curing is highly important, and many attempts have been conducted. Sudo et al. [46] investigated the substituent effects of N-alkyl groups on thermally induced curing behaviour and found that N-methylbenzoxazine with the smallest alkyl group underwent the fastest curing. Martos et al. [47] prepared several substituted monobenzoxazines at the para and meta positions of the phenolic ring and studied how these substituents affected the curing temperature of benzoxazine. It was observed that the presence of substituents in the meta position had a greater effect on decreasing the curing temperature, and when the substituent was fluorine the decrease was more than 40°C. The findings of Kolanadiyil et al. [48] suggested that when the benzoxazine monomer was substituted with another benzoxazine moiety instead of another functional group, meta-substitution resulted in a lower curing temperature and more favourable properties than the ortho- and para-substituted counterparts due to the shorter intramolecular interaction distance. Lyu and coworkers [49] studied the effects of asymmetric and meta-alkoxy substituents on the curing behaviour of bis-benzoxazines, which showed that when the substituent group was at the 7-position of the benzoxazine ring the bis-benzoxazine had a lower curing temperature than when the substituent group was at the 5-position, even though the substituents were all at the meta position of phenol group. It has also been found that electron-withdrawing groups led to a more acidic phenolic species, resulting in a stronger catalytic effect and an expected trend of benzoxazine ring opening. Wang et al. [50] investigated the influence of electronic effects of the bridging groups on the ring-forming reaction and thermally activated curing, with the results showing that electron-withdrawing groups lowered the curing energy barrier and resulted in a lower curing temperature.

However, there have also been some different and even opposite research conclusions. Andreu et al. [51] found that if the substituent was electron withdrawing it would lead to a low curing temperature when in the para position of phenol group, while it would lead to an increase in curing temperature when in the para position of the amine group. They also found that—except for the phenol group—electron-donating substituents had no significant effect on the reaction temperature no matter where they were located [52]. Martos et al. found no apparent trend in the curing of differently substituted 3-phenyl-3,4-dihydro-2H-1,3-benzoxazines, with both electron-withdrawing and electron-donating groups being capable of accelerating the curing process [53].

Therefore, the influence of substituents—especially electron-donating groups—on the curing process of benzoxazine monomers is still not fully understood. Additionally, there have been few studies on the thermal curing of bio-based benzoxazines, which is very important for informing the design of their molecular structure [9,54–58]. Therefore, the influence of substituents on the thermal curing of bio-based benzoxazines was the focus of the present study.

Inspired by the extensive research on benzoxazines by our research group over many years, in this study, several new bio-based benzoxazines with different substituent groups were synthesized and their curing characteristics were studied. The purpose of this study was to deepen understanding of the influence of substituent steric and electronic effects on the curing properties of bio-based benzoxazines.

## 2 Experimental

## 2.1 Materials

All reagents, including furfuryl amine, octadecylamine, polyoxymethylene, carvacrol, 5-methyl-2-isopropylphenol, o-methyl phenol, m-methyl phenol, o-chlorophenol and sodium bicarbonate were purchased from Millipore Sigma Co., Germany and used without any further purification. Dioxane was purchased from Shanghai Aladdin Biochemical Technology Co. Ltd., Shanghai, China. Solvents were reagent grade.

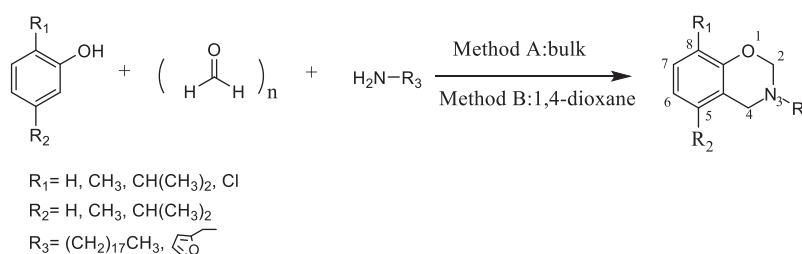
The main raw materials of this paper, such as furfuryl amine [59–62], octadecylamine [63], carvacrol [64,65], 5-methyl-2-isopropylphenol [66,67], o-methylphenol [68], m-methylphenol [69] can be prepared from biological sources, and there have industrial products. This shows that we can use biological raw materials to prepare the benzoxazines in this study.

## 2.2 Characterization

The molecular structure of the benzoxazine was analyzed by nuclear magnetic resonance (NMR) spectroscopy. <sup>1</sup>H-NMR and <sup>13</sup>C-NMR spectra were recorded on an AVANCW 600 spectrometer with Fourier transform, with CDCl<sub>3</sub> and DMSO-d<sub>6</sub> as solvents and TMS as an internal standard. Calorimetric studies were performed using a Diamond differential scanning calorimetry (DSC) thermal analyzer with N<sub>2</sub> as the purge gas at different scanning rates of 5, 10, 15 and 20 °C/min. The quantum chemical calculations of the molecules m<sub>1</sub>-m<sub>8</sub> were performed by using Gaussian 09W software programs on a AMD A4-5000 APU with Radeon(TM) HD Graphics/1.50GHz personal computer. The molecular structure of the investigated compounds in the ground state was optimized using Density Functional Theory (DFT) method (functional B3LYP ). The electronic properties such as energies HOMO(Highest Occupied Molecular) and LUMO(Lowest Unoccupied Molecular) orbitals, energy gap between LUMO and HOMO (HOMO-LUMO = E<sub>LUMO</sub> – E<sub>HOMO</sub>) were carried out using the B3LYP/6-31g(d,p) levels of theory. HOMO, LUMO were visualized using GaussView 6.0 program.

### 2.3 Synthesis of Benzoxazine

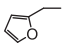
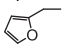
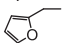
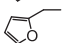
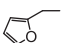
The bio-based benzoxazines were synthesized according to [Scheme 1](#), with their names and chemical structures listed in [Tab. 1](#). The corresponding  $^1\text{H}$ -NMR and  $^{13}\text{C}$ -NMR spectra are provided in the Appendix.



**Scheme 1: Synthesis of benzoxazine**

Two synthetic methods, solvent and solvent-free method, are used. Take a certain amount of phenolic, amine and paraformaldehyde (the ratio of phenolic, amine and paraformaldehyde is 1:1:2) into the reactor. Dioxane was added as the solvent if solvent method is used. The reaction temperature was 90°C and the reaction time was 12 h. Then the reaction system is cooled to room temperature and a vacuum distillation solvent is placed on a rotary evaporator. The remaining solids are washed in a hot sodium bicarbonate solution until the water layer becomes transparent. The product was washed to neutral with deionized water and a few drops of ethanol were added to the wash solution. After filtration and liquid separation, the products were dried in vacuum drying oven at 65°C for 24 h.

**Table 1:** Structure and melting point of benzoxazine

Sample	R <sub>1</sub>	R <sub>2</sub>	R <sub>3</sub>	Melting point (°C)
m <sub>0</sub> <sup>*</sup>	H	H	Ph	56.5
m <sub>1</sub>	CH <sub>3</sub>	CH(CH <sub>3</sub> ) <sub>2</sub>	(CH <sub>2</sub> ) <sub>17</sub> CH <sub>3</sub>	40.1
m <sub>2</sub>	CH(CH <sub>3</sub> ) <sub>2</sub>	CH <sub>3</sub>	(CH <sub>2</sub> ) <sub>17</sub> CH <sub>3</sub>	39.3
m <sub>3</sub>	CH <sub>3</sub>	CH(CH <sub>3</sub> ) <sub>2</sub>		63.9
m <sub>4</sub>	CH(CH <sub>3</sub> ) <sub>2</sub>	CH <sub>3</sub>		liquid (25°C)
m <sub>5</sub>	CH <sub>3</sub>	H		liquid (25°C)
m <sub>6</sub>	H	CH <sub>3</sub>		39.8
m <sub>7</sub>	H	CH <sub>3</sub>	(CH <sub>2</sub> ) <sub>17</sub> CH <sub>3</sub>	44.7
m <sub>8</sub>	Cl	H		liquid (25°C)

Note: <sup>\*</sup>Data are quoted from [49].

### 2.3.1 3, 4-dihydro-3-octadecyl -2H-6-isopropyl-9-methyl-1, 3-benzoxazine(m<sub>1</sub>)

carvacrol (50 mmol, 7.511 g), Octadecylamine (50 mmol, 13.476 g) and paraformaldehyde (100 mmol, 3 g) were weighed in the reactor and added with 200 mL dioxane as the solvent. Yield 67%. Melting point 40.1°C. <sup>1</sup>H-NMR and <sup>13</sup>C-NMR spectrum are shown in Fig. S1. The data of <sup>1</sup>H-NMR and <sup>13</sup>C-NMR are as follows:

<sup>1</sup>H-NMR(CDCl<sub>3</sub>,TMS,ppm):6-7(H,Ar-H),4.83(2H,O-CH<sub>2</sub>-N),4.00(2H,Ar-CH<sub>2</sub>-N),2.70(1H,CH),2.14(3H,Ar-CH<sub>3</sub>),1.20(6H,CH<sub>3</sub>),0.8-2.7(37H,CH<sub>2</sub>);<sup>13</sup>C-NMR(CDCl<sub>3</sub>,TMS,ppm):116-152(Ar-C),81.46(O-CH<sub>2</sub>-N),51.69(Ar-CH<sub>2</sub>-N),48.11(N-CH<sub>2</sub>),14-32(CH<sub>2</sub>),23.58(CH),27.83(CH<sub>3</sub>),15.72(Ar-CH<sub>3</sub>).

### 2.3.2 3, 4-dihydro-3-octadecyl -2H-6-methyl-9-isopropyl-1, 3-benzoxazine (m<sub>2</sub>)

5-methyl-2-Isopropylphenol (50 mmol, 7.511 g),Octadecylamine (50 mmol, 13.476 g) and paraformaldehyde (100 mmol, 3 g) were weighed in the reactor and add 200 mL dioxane as the solvent. Yield 74%. Melting point 39.3°C. <sup>1</sup>H-NMR and <sup>13</sup>C-NMR spectrum are shown in Fig. S2. The data of <sup>1</sup>H-NMR and <sup>13</sup>C-NMR are as follows:

<sup>1</sup>H-NMR(CDCl<sub>3</sub>,TMS,ppm):6-7(H,Ar-H),4.81(2H,O-CH<sub>2</sub>-N),3.87(2H,Ar-CH<sub>2</sub>-N),3.22(1H,CH),2.12(3H,Ar-CH<sub>3</sub>),0.88(6H,CH<sub>3</sub>),0.8-2.8(37H,CH<sub>2</sub>);<sup>13</sup>C-NMR(CDCl<sub>3</sub>,TMS,ppm):118-152(Ar-C),81.70(O-CH<sub>2</sub>-N),51.75(Ar-CH<sub>2</sub>-N),49.28(N-CH<sub>2</sub>),14-33(CH<sub>2</sub>),22.96(CH),28.20(CH<sub>3</sub>),17.76(Ar-CH<sub>3</sub>).

### 2.3.3 3, 4-dihydro-3-methylene furan-2H-6-isopropyl-9-methyl-1, 3-benzoxazine(m<sub>3</sub>)

carvacrol (50 mmol, 7.511 g), Furfuryl amine (50 mmol, 4.856 g) and paraformaldehyde (100 mmol, 3 g) were weighed in the reactor. Yield 85%. Melting point 63.9°C. <sup>1</sup>H-NMR and <sup>13</sup>C-NMR spectrum are shown in Fig. S3. The data of <sup>1</sup>H-NMR and <sup>13</sup>C-NMR are as follows:

<sup>1</sup>H-NMR(CDCl<sub>3</sub>,TMS,ppm):7.42(1H,O-CH=C),6.34(1H,C=CH),6.22(1H,C=CH),6-7(H,Ar-H),4.90(2H,O-CH<sub>2</sub>-N),4.02(2H,Ar-CH<sub>2</sub>-N),3.93(2H,CH<sub>2</sub>),2.78(1H,CH),2.17(3H,Ar-CH<sub>3</sub>),1.16(6H,CH<sub>3</sub>);<sup>13</sup>C-NMR(CDCl<sub>3</sub>,TMS,ppm):108-152(Ar-C),108.94(C=CH),110.21(C=CH),151.87(O-CH=C),81.32(O-CH<sub>2</sub>-N),48.58(Ar-CH<sub>2</sub>-N),47.22(N-CH<sub>2</sub>),23.34(CH),28.28(CH<sub>3</sub>),15.51(Ar-CH<sub>3</sub>).

### 2.3.4 3, 4-dihydro-3-methylene furan-2H-6-methyl-9-isopropyl-1, 3-benzoxazine(m<sub>4</sub>)

5-methyl-2-Isopropylphenol (50 mmol, 7.511 g), Furfuryl amine (50 mmol, 4.856 g) and paraformaldehyde (100 mmol, 3 g) were weighed in the reactor. Yield 87%. <sup>1</sup>H-NMR and <sup>13</sup>C-NMR spectrum are shown in Fig. S4. The data of <sup>1</sup>H-NMR and <sup>13</sup>C-NMR are as follows:

$^1\text{H-NMR}(\text{CDCl}_3, \text{TMS}, \text{ppm}): 7.40(1\text{H}, \text{O-CH}=\text{C}), 6.32(1\text{H}, \text{C}=\text{CH}), 6.24(1\text{H}, \text{C}=\text{CH}), 6-7(\text{H}, \text{Ar-H}), 4.86(2\text{H}, \text{O-CH}_2\text{-N}), 3.81(4\text{H}, \text{Ar-CH}_2\text{-N}, \text{CH}_2), 3.26(1\text{H}, \text{CH}), 2.08(3\text{H}, \text{Ar-CH}_3), 1.22(6\text{H}, \text{CH}_3); ^{13}\text{C-NMR}(\text{CDCl}_3, \text{TMS}, \text{ppm}): 105-152(\text{Ar-C}, \text{C}=\text{CH}, \text{O-CH}=\text{C}), 81.18(\text{O-CH}_2\text{-N}), 48.60(\text{Ar-CH}_2\text{-N}), 48.16(\text{N-CH}_2\text{-}), 22.70(\text{CH}), 26.47(\text{CH}_3), 18.03(\text{Ar-CH}_3).$

### 2.3.5 3, 4-dihydro-3-methylene furan-2H-9-methyl-1, 3-benzoxazine( $m_5$ )

o-methyl phenol (50 mmol, 5.406 g), Furfuryl amine (50 mmol, 4.856 g) and paraformaldehyde (100 mmol, 3 g) were weighed in the reactor. Yield 85%.  $^1\text{H-NMR}$  and  $^{13}\text{C-NMR}$  spectrum are shown in Fig. S5. The data of  $^1\text{H-NMR}$  and  $^{13}\text{C-NMR}$  are as follows:

$^1\text{H-NMR}(\text{CDCl}_3, \text{TMS}, \text{ppm}): 6-7(\text{H}, \text{Ar-H}), 4.92(2\text{H}, \text{O-CH}_2\text{-N}), 3.99(2\text{H}, \text{Ar-CH}_2\text{-N}), 3.92(2\text{H}, \text{CH}_2), 2.19(3\text{H}, \text{Ar-CH}_3); ^{13}\text{C-NMR}(\text{CDCl}_3, \text{TMS}, \text{ppm}): 108-152(\text{Ar-C}, \text{C}=\text{CH}, \text{O-CH}=\text{C}), 81.20(\text{O-CH}_2\text{-N}), 49.80(\text{Ar-CH}_2\text{-N}), 48.76(\text{N-CH}_2), 18.74(\text{Ar-CH}_3).$

### 2.3.6 3, 4-dihydro-3-methylene furan-2H-6-methyl-1, 3-benzoxazine( $m_6$ )

m-ethylene phenol (50 mmol, 5.406 g), Furfuryl amine (50 mmol, 4.856 g) and paraformaldehyde (100 mmol, 3 g) were weighed in the reactor. Yield 82%. Melting point  $39.8^\circ\text{C}$ .  $^1\text{H-NMR}$  and  $^{13}\text{C-NMR}$  spectrum are shown in Fig. S6. The data of  $^1\text{H-NMR}$  and  $^{13}\text{C-NMR}$  are as follows:

$^1\text{H-NMR}(\text{CDCl}_3, \text{TMS}, \text{ppm}): 6-7(\text{H}, \text{Ar-H}), 4.87(2\text{H}, \text{O-CH}_2\text{-N}), 3.92(2\text{H}, \text{Ar-CH}_2\text{-N}), 3.98(2\text{H}, \text{CH}_2), 2.28(3\text{H}, \text{Ar-CH}_3); ^{13}\text{C-NMR}(\text{CDCl}_3, \text{TMS}, \text{ppm}): 106-155(\text{Ar-C}, \text{C}=\text{CH}, \text{O-CH}=\text{C}), 82.30(\text{O-CH}_2\text{-N}), 48.90(\text{Ar-CH}_2\text{-N}), 49.34(\text{N-CH}_2), 16.74(\text{Ar-CH}_3).$

### 2.3.7 3, 4-dihydro-3-octadecyl -2h-6-methyl-1, 3-benzoxazine( $m_7$ )

m-ethylene phenol (50 mmol, 5.406 g), Octadecylamine (50 mmol, 13.476 g) and paraformaldehyde (100 mmol, 3 g) were weighed in the reactor and added with 200 mL dioxane as the solvent. Yield 73%. Melting point  $44.7^\circ\text{C}$ .  $^1\text{H-NMR}$  and  $^{13}\text{C-NMR}$  spectrum are shown in Fig. S7. The data of  $^1\text{H-NMR}$  and  $^{13}\text{C-NMR}$  are as follows:

$^1\text{H-NMR}(\text{CDCl}_3, \text{TMS}, \text{ppm}): 6-7(\text{H}, \text{Ar-H}), 4.86(2\text{H}, \text{O-CH}_2\text{-N}), 3.69(2\text{H}, \text{Ar-CH}_2\text{-N}), 2.21(3\text{H}, \text{Ar-CH}_3), 0.8-2.7(37\text{H}, \text{CH}_2); ^{13}\text{C-NMR}(\text{CDCl}_3, \text{TMS}, \text{ppm}): 117-162(\text{Ar-C}), 82.58(\text{O-CH}_2\text{-N}), 51.39(\text{Ar-CH}_2\text{-N}), 14-32(\text{CH}_2), 14.20(\text{Ar-CH}_3).$

### 2.3.8 3, 4-dihydro-3-methylene furan-2H-9-chloro-1, 3-benzoxazine( $m_8$ )

O-Chlorophenol (50 mmol, 6.428 g), Furfuryl amine (50 mmol, 4.856 g) and paraformaldehyde (100 mmol, 3 g) were weighed in the reactor. Yield 93%.  $^1\text{H-NMR}$  and  $^{13}\text{C-NMR}$  spectrum are shown in Fig. S8. The data of  $^1\text{H-NMR}$  and  $^{13}\text{C-NMR}$  are as follows:

$^1\text{H-NMR}(\text{CDCl}_3, \text{TMS}, \text{ppm}): 6-7.3(\text{H}, \text{Ar-H}), 5.02(2\text{H}, \text{O-CH}_2\text{-N}), 4.01(2\text{H}, \text{Ar-CH}_2\text{-N}), 3.93(2\text{H}, \text{N-CH}_2); ^{13}\text{C-NMR}(\text{CDCl}_3, \text{TMS}, \text{ppm}): 108-155(\text{Ar-C}, \text{C}=\text{CH}, \text{O-CH}=\text{C}), 81.91(\text{O-CH}_2\text{-N}), 48.22(\text{Ar-CH}_2\text{-N}), 49.54(\text{N-CH}_2).$

## 3 Results and Discussion

### 3.1 Curing Kinetics of Benzoxazine Monomers

The Kissinger and Ozawa methods [70] were used to calculate the curing reaction activation energy of benzoxazine. The basic assumptions of the curing process were as follows: (1) the highest curing rate occurred at the peak temperature; (2) the simple n-order reaction remained unchanged during curing. The Kissinger and Ozawa equations are shown below as Eqs. (1) and (2), respectively.

$$\ln\left(\frac{\beta}{T_p^2}\right) = \ln\frac{AR}{E_a} - \frac{E_a}{RT_p} \quad (1)$$

$$\ln\beta = C - 1.052 \frac{E_a}{RT_p} \quad (2)$$

Here,  $T_p$  (K) is the peak curing temperature obtained from the DSC curve;  $\beta$  ( $\text{K}\cdot\text{min}^{-1}$ ) is the heating rate;  $A$  is the apparent coefficient of curing; and  $E_a$  is the apparent activation energy. The Kissinger method assumes that the curing is an  $n$ -order reaction from beginning to end, while the Ozawa method calculates activation energy without considering the reaction mechanism.

The exothermic peaks during curing of bio-based benzoxazine with different substituent groups at different heating rates can be observed from Fig. 1. The  $^1\text{H}$ -NMR and  $^{13}\text{C}$ -NMR data in supporting information proved that the benzoxazines were of high purity because there are no hetero peaks in the NMR spectra. So all DSC curves at different heating rates had only one exothermic peak. In addition, it was found that with increased heating rate, the exothermic peak moved to a higher temperature. This was mainly due to the delayed curing effect at high heating rates.

The curing activation energies of  $m_1$ - $m_8$  calculated by the Kissinger and Ozawa methods are shown in Figs. 2, 3, Tab. 2. It can be inferred from the data in Tab. 2 that the curing reaction order for all benzoxazines was about 1. And the HOMO-LUMO values were performed on Gaussian 09W.

### 3.2 The Influence of Spatial and Electronic Effects on the Curing Temperature of Benzoxazine

We focused on the activation energy values calculated by the Ozawa method, because this method is independent of the curing mechanism and so avoids errors due to different assumptions of reaction mechanism functions [70]. The ring-opening curing temperatures and the curing reaction activation energies of the differently-substituted benzoxazines are listed in Tab. 2. It was found that the benzoxazines with lower ring-opening temperature had lower activation energy, which was consistent with traditional research results.

Both the spatial and electronic effects of substituents can affect the thermal curing temperature of benzoxazine. When the substituent groups were located at different positions on benzoxazine they had different effects. For example, when the  $R_3$  group was directly connected to the nitrogen atom of the benzoxazine ring it had mainly a steric hindrance effect during curing. The chemical structures of  $m_1$  and  $m_3$  differed only in terms of the  $R_3$  group: the  $R_3$  group of  $m_1$  was bigger than that of  $m_3$ , which resulted in  $m_1$  having a higher curing activation energy and higher curing temperature than  $m_3$ . The simulated conformations of these benzoxazines (Fig. 4) show the bulkiness of the different  $R_3$  groups. The octadecyl and furan ring moieties are both electron-rich groups but have different bulkiness and different steric hindrance. The  $m_1$  compound contained an octadecyl  $R_3$  group with greater steric hindrance than that of the furan ring  $R_3$  group in  $m_3$ , and the peak curing temperature ( $T_p$ ) of  $m_1$  was greater by about  $70^\circ\text{C}$ .

Comparison of  $m_2$  and  $m_4$ , as well as  $m_6$  and  $m_7$ , enabled the same conclusion to be made, that is, the larger the  $R_3$  group the greater its steric hindrance, and the more obvious its inhibition effect on the curing process, resulting in a greater increase in the curing temperature. The possible reason for this is related to the curing mechanism of benzoxazine, as shown in Scheme 2. The thermal curing of benzoxazine is a cationic ring-opening reaction due to the presence of oxygen atoms. First, the C-O bond in the oxazine ring  $\text{Ar-O-CH}_2$  structure breaks to form  $\text{O}^-$  and carbocation  $^+\text{CH}_2$ , and then the carbocation in structure b attacks the para-position crosslinking point of the phenolic hydroxyl to achieve the polymerisation chain growth reaction of polybenzoxazine. When the volume of  $R_3$  group was larger, the steric hindrance carried by the carbocation was larger, which increased the curing temperature.



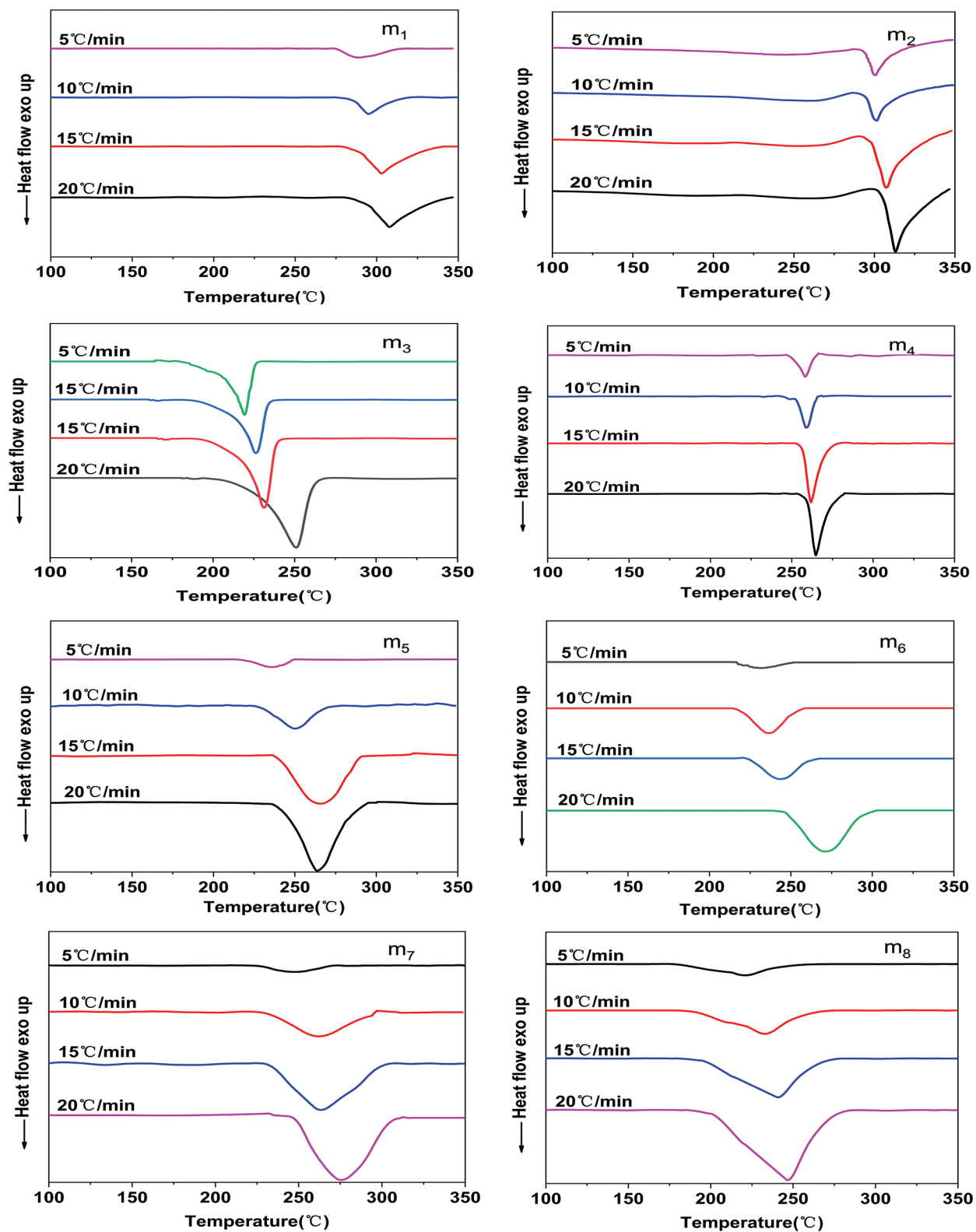
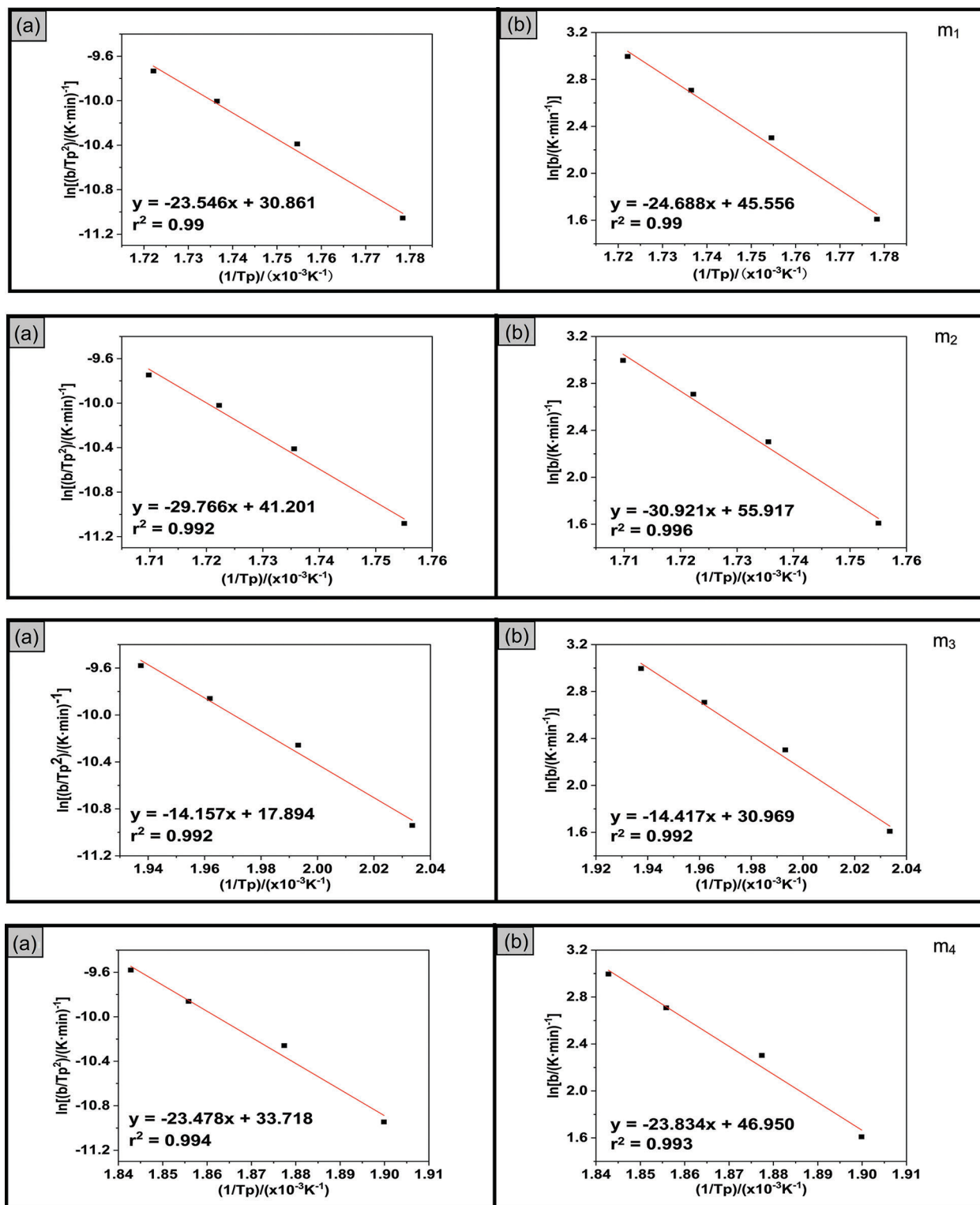
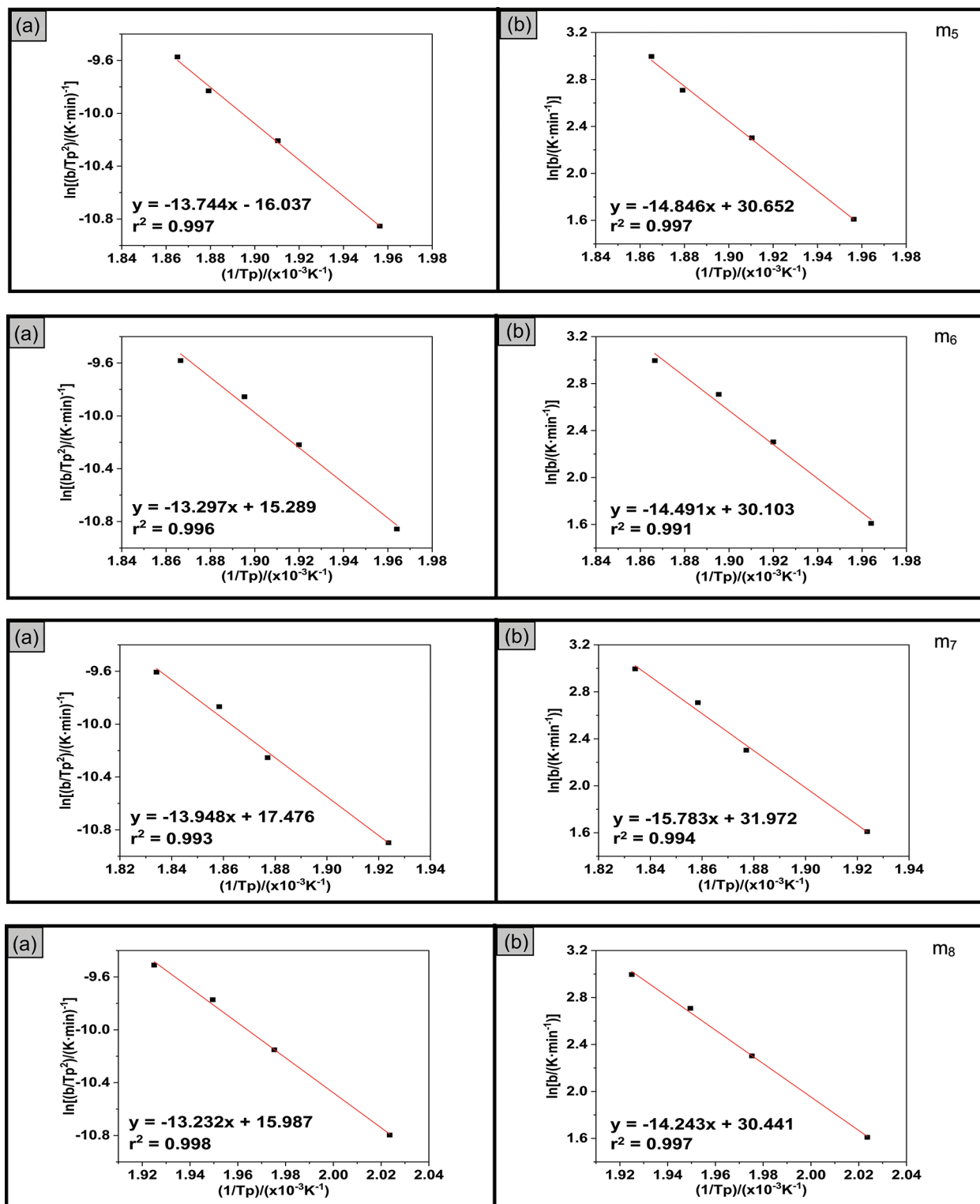


Figure 1: DSC spectra of the curing of benzoxazine ( $m_1$ – $m_8$ )



**Figure 2:** Fitting results of  $m_1$ – $m_4$ : (a) Kissinger plot of  $\ln(\beta/T_p^2)$  vs.  $1/T_p$ ; (b) Ozawa plot of  $\ln\beta$  vs.  $1/T_p$

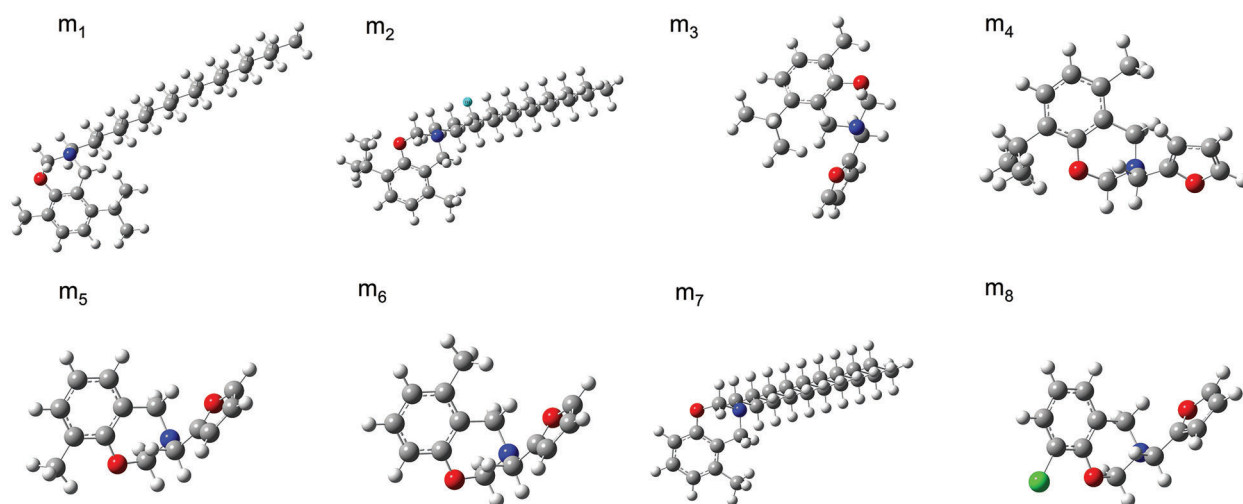
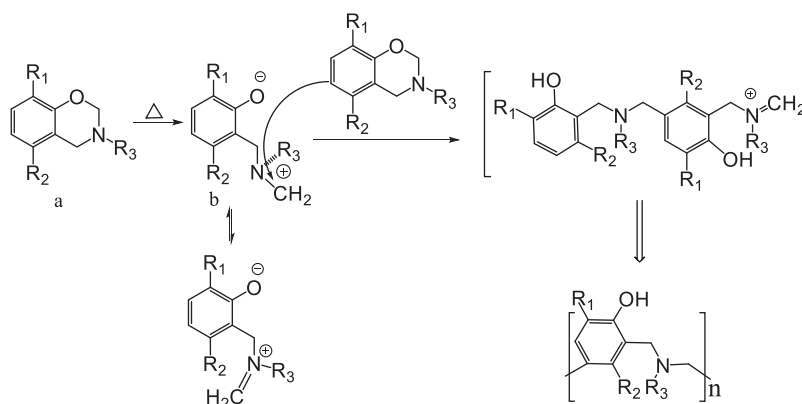




**Figure 3:** Fitting results of m<sub>5</sub>–m<sub>8</sub>: (a) Kissinger plot of  $\ln(\beta/T_p^2)$  vs.  $1/T_p$ ; (b) Ozawa plot of  $\ln\beta$  vs.  $1/T_p$

**Table 2:** Curing temperature and activation energy of benzoxazine monomers

	T <sub>o(onset)</sub> (°C)	T <sub>p(peak)</sub> (°C)	E <sub>Kissinger</sub> (kJ·mol <sup>-1</sup> )	E <sub>Ozawa</sub> (kJ·mol <sup>-1</sup> )	LUMO (a.u.)	HOMO (a.u.)	HOMO-LUMO (a.u.)
m <sub>0</sub> <sup>*</sup>	263.5	267.9	—	—	—	—	—
m <sub>1</sub>	275.0	289.2	195.76	195.11	0.0024	-0.2083	0.2107
m <sub>2</sub>	289.2	296.6	247.47	244.37	0.0017	-0.2091	0.2108
m <sub>3</sub>	170.4	221.3	117.71	113.94	0.0037	-0.2072	0.2109
m <sub>4</sub>	246.9	259.1	195.20	185.50	0.0057	-0.2083	0.2140
m <sub>5</sub>	217.1	236.1	114.27	117.33	0.0013	-0.2097	0.2110
m <sub>6</sub>	217.0	235.4	110.55	114.53	0.0037	-0.2105	0.2142
m <sub>7</sub>	225.3	246.7	115.96	124.73	0.0030	-0.2123	0.2153
m <sub>8</sub>	180.16	221.0	110.01	112.56	-0.0123	-0.2151	0.2028

Note: <sup>\*</sup>Data are quoted from [53].**Figure 4:** Simulated spatial conformations of model monomers**Scheme 2:** Proposed mechanism for the thermal curing of benzoxazines

There is also another potential explanation for this phenomenon: the electronic effect. Under this interpretation, since the electron-donating capacity of octadecyl is weaker than that of the furan ring, the curing temperature of benzoxazine substituted by the former was higher than that of the latter. However, comparison of  $m_1$  and  $m_3$  did not reveal an obvious electronic effect difference arising from the presence of the octadecyl versus furan ring, but the difference in  $T_p$  was so great that we doubt whether the electronic effect can be used to explain this phenomenon. Therefore, the HOMO-LUMO difference of the benzoxazines was calculated and simulated (Tab. 2). The greater the energy level difference, the greater the energy required for electronic transition, and therefore the larger the activation energy and the higher the temperature required for curing. This value was only used to compare the electronic effect and does not consider any spatial effects.

According to the calculated HOMO-LUMO values, the order of  $T_p$  should be  $m_1 < m_3$ ,  $m_2 < m_4$  and  $m_6 > m_7$ , but the actual measured data was the opposite. This indicated that the difference in curing temperature between these three groups was not mainly caused by the electronic effect, but by the spatial effect mentioned above. In fact, considering the position of the  $R_3$  group and the curing mechanism, we speculate that the  $R_3$  group in the benzoxazine monomer is too far away from the crosslinking point, so the electron induction effect is very weak and only the steric hindrance effect has any impact at the  $R_3$  position.

The  $R_1$  and  $R_2$  groups on the benzene ring also showed spatial effects. According to the theoretical curing mechanism (Scheme 2), when substituents are located in the  $R_2$  position and  $R_1$  position they will have a considerable spatial effect as both positions are closer to the crosslinking point than other positions on the benzene ring. In other words, if a larger substituent is located in the  $R_1$  or  $R_2$  position, it will obviously increase the curing temperature.

The  $m_2$  and  $m_7$  compounds had the same  $R_2$  and  $R_3$  groups but a different  $R_1$  group. It can be seen from Tab. 2 that  $m_2$ , which had a larger  $R_1$  group, had a higher curing temperature than  $m_7$ . The same trend was found when comparing  $m_4$  and  $m_6$  (which had the same  $R_2$  and  $R_3$  groups but a different  $R_1$  group). There was also a difference in curing temperature for  $m_1$  and  $m_7$ , which had different-sized groups in the  $R_2$  position, and the curing temperature was  $m_1 > m_7$ . These results showed that the larger the  $R_1$  and  $R_2$  groups, the greater the steric hindrance around the crosslinking point and the higher the curing temperature.

There was also another phenomenon that attracted our attention. It appeared that even the same substituent group, when it was located at different positions, had different influences on the curing reaction. For example, if only considering the spatial effect, the  $T_p$  of  $m_2$  should be higher than that of  $m_7$  because  $m_2$  had the same  $R_2$  substituent as  $m_7$  and a larger  $R_1$  substituent than  $m_7$ . For the same reason, if there was just a spatial effect at the  $R_2$  position, the  $T_p$  of  $m_3$  should be higher than that of  $m_5$  because  $m_3$  had the same  $R_1$  substituent as  $m_5$  and a larger  $R_2$  substituent than  $m_5$ . Similarly, if only considering the electronic effect, the  $T_p$  of  $m_2$  should be lower than that of  $m_7$  because the HOMO-LUMO value of  $m_2$  was smaller. For the same reason, the  $T_p$  of  $m_3$  should be lower than that of  $m_5$ . Therefore, it seemed that the conclusions based on electronic effects and the conclusions based on spatial effects were contradictory. Furthermore, the  $T_p$  of  $m_2$  was markedly higher than that of  $m_7$  while the  $T_p$  of  $m_3$  was slightly higher than that of  $m_5$ . This indicated that not only steric hindrance effects but also electronic effects of the  $R_1$  and  $R_2$  groups should be considered during curing.

To investigate this further, we first studied the effect of the  $R_1$  substituent group on curing. As an example,  $m_0$ —which had no substituents at the  $R_1$  and  $R_2$  positions—had a  $T_p$  of 267.9°C while the  $T_p$  of  $m_8$ , which contained a chlorine atom at  $R_1$ , was 221°C, and the  $T_p$  of  $m_3$  with a substituent at both  $R_1$  and  $R_2$  was 221.3°C. This meant that there was an influence from the electronic effect, and to a some extent this effect was more important than spatial effect.

The results of  $m_5$  with  $m_8$ , which had similar structures but  $R_1$  groups that were similar in bulk but opposite in electron negativity, were compared. It could be seen that  $m_8$ , which had an electron-withdrawing  $R_1$  group,

had a lower  $T_p$  than that of  $m_5$ , which had an electron-donating  $R_1$  group. The HOMO-LUMO value of  $m_8$  was also lower than that of  $m_5$ . In another example,  $m_0$  had the smallest spatial effect and  $m_8$  had a larger but electron-withdrawing  $R_1$  group, but the  $T_p$  of  $m_0$  was higher than that of  $m_8$ . Furthermore,  $m_2$  had a larger and stronger electron-donating  $R_1$  group than  $m_7$ , so it has a higher  $T_p$  than  $m_5$ , in this case, the steric hindrance effect and the electronic effect reinforced each other.

These results indicated that the electronic effect of the  $R_1$  group was stronger its spatial effect on the curing of benzoxazine: an electron-withdrawing  $R_1$  group will promote the curing reaction of benzoxazine, while an electron-donating  $R_1$  group will inhibit the curing reaction. There are two possible explanations for this. First, electron-withdrawing substituents decrease the electron cloud density of  $O^-$  on the oxazine ring, making the C-O bond easier to break. Second, electron-withdrawing substituents can form more acidic phenols and increase the acidity of the phenolic hydroxyl group after ring opening, thus generating a stronger auto-catalytic effect. Conversely, electron-donating groups do not promote the formation of  $O^-$  and C-O bond fracture. It has also been widely reported that electron-withdrawing groups can promote the curing reaction of benzoxazine [36,71].

To study the influence of the  $R_2$  group, the  $T_p$  values of  $m_3$  and  $m_5$  were compared. There was only one difference between them:  $m_3$  had a large and stronger electron-donating  $R_2$  group. Although the  $R_2$  group in  $m_3$  was more electron-donating and had great steric hindrance, the  $T_p$  of  $m_3$  was lower than that of  $m_5$ . This was a different trend to that observed for the effect of the  $R_1$  group: for the  $R_1$  group, electron-donating groups hindered curing, but for the  $R_2$  group, electron-donating substituents promoted the ring-opening curing process.

Furthermore, results of  $m_1$  and  $m_2$ , and  $m_3$  and  $m_4$ , were compared. These two pairs of compounds had the same characteristic: they contained the same  $R_1$  and  $R_2$  groups, but their positions were interchanged. Tab. 2 shows that for both groups, when the electron-donating property of  $R_2$  group was stronger the benzoxazine had a lower curing temperature, while the spatial effect was not prominent. Theoretical calculations also verified this point: the HOMO-LUMO values were  $m_1 < m_2$  and  $m_3 < m_4$ ; this indicated whether the energy required for electron transition was large or small, and whether the  $T_p$  of the corresponding benzoxazine was high or low. Considering the curing mechanism (Scheme 2), since electron-donating groups increase the electron cloud density of the ortho-crosslinking site, this facilitates electrophilic substitution via attack of  $^+CH_2$  on the crosslinking reaction centre. This was consistent with the experimental results shown in Tab. 2.

Overall, we could conclude that the electronic effect of the  $R_3$  group was secondary and its steric hindrance effect was more important in the curing of benzoxazine. For the  $R_1$  and  $R_2$  groups, they all showed a certain steric hindrance effect, but because they were closer to the crosslinking reaction centre their electronic effect had a greater influence on the curing reaction than their spatial effect. Additionally, because the  $R_1$  group is close to the  $O^-$  reaction site, when  $R_1$  was an electron-withdrawing group its promoting effect on the reaction was more obvious than when  $R_3$  was an electron-donating group. And because the  $R_2$  group was closer to the  $^+CH_2$  reaction site, when  $R_2$  was an electron-donating group it had a marked promoting effect on the curing reaction.

It has been widely reported that electron-withdrawing groups can promote the curing reaction, but our study indicated that this conclusion is limited to the group at the  $R_1$  position. In fact, when an electron-donating group is at the  $R_2$  position is, it will also promote the curing reaction. Although more model compounds and more in-depth studies are needed to obtain more accurate conclusions, this study increases understanding of how spatial and electronic effects play different roles in the different positions.

#### 4 Conclusion

In this study, eight kinds of bio-based benzoxazine monomers with different substituent groups were successfully prepared, and their structures were characterized by NMR. The curing of these bio-based

benzoxazine monomers was studied using the non-isothermal DSC method. The results showed that the curing reaction kinetics of each monomer conformed to the first-order kinetic model, making the peak temperatures of the curing reactions comparable. By comparing the reaction activation energy and curing temperature, the following observations were made. (1) For the R<sub>3</sub> position, it was mainly the steric hindrance effect that influenced the curing process, with bulkier substituents having a more obvious inhibitory effect on the ring-opening process and leading to a higher T<sub>p</sub>. (2) For the R<sub>1</sub> and R<sub>2</sub> positions there was not only a spatial effect but also an electronic effect that influenced the curing of benzoxazine. When R<sub>1</sub> was an electron-withdrawing group it had a marked promoting effect on the curing reaction; when R<sub>1</sub> was an electron-donating group it had an inhibitory effect. When R<sub>2</sub> was an electron-donating group it had a marked promoting effect on curing reaction. The influence of electronic effects was also verified by theoretical calculations.

The findings of this study help increase the understanding of how spatial and electronic effects have different impacts in different substituent positions.

**Funding Statement:** This work was partially supported by the National Natural Science Foundation of China (51773060, and 52073091), Shanghai Natural Science Foundation (20ZR1414600), Shanghai Aerospace Science and Technology Innovation Fund (SAST2020-087), and the Fundamental Research Funds for the Central Universities (50321042017001).

**Conflicts of Interest:** The authors declare that they have no conflicts of interest to report regarding the present study.

## References

1. Li, X., Luo, X., Liu, M., Ran, Q., Gu, Y. (2014). The catalytic mechanism of benzoxazine to the polymerization of cyanate ester. *Materials Chemistry and Physics*, 148(1–2), 328–334. DOI 10.1016/j.matchemphys.2014.07.051.
2. Sawaryn, C., Landfester, K., Taden, A. (2011). Cationic polybenzoxazines. A novel polyelectrolyte class with adjustable solubility and unique hydrogen-bonding capabilities. *Macromolecules*, 44(19), 7668–7674. DOI 10.1021/ma201414t.
3. Arslan, M., Kiskan, B., Yagci, Y. (2018). Benzoxazine-based thermoset with autonomous self-healing and shape recovery. *Macromolecules*, 51(24), 10095–10103. DOI 10.1021/acs.macromol.8b02137.
4. Puchot, L., Verge, P., Fouquet, T., Vancaeyzeele, C., Vidal, F. et al. (2016). Breaking the symmetry of dibenzoxazines: A paradigm to tailor the design of bio-based thermosets. *Green Chemistry*, 18(11), 3346–3353. DOI 10.1039/C5GC03102H.
5. He, Y., Gao, S., Lu, Z. (2018). A mussel-inspired polybenzoxazine containing catechol groups. *Polymer*, 158(3), 53–58. DOI 10.1016/j.polymer.2018.10.046.
6. He, Y., Gao, S., Jubsilp, C., Rimdusit, S., Lu, Z. (2020). Reprocessable polybenzoxazine thermosets crosslinked by mussel-inspired catechol-Fe<sup>3+</sup> coordination bonds. *Polymer*, 192(1), 122307. DOI 10.1016/j.polymer.2020.122307.
7. Han, L., Zhang, K., Ishida, H., Froimowicz, P. (2017). Study of the effects of intramolecular and intermolecular hydrogen-bonding systems on the polymerization of amide-containing benzoxazines. *Macromolecular Chemistry and Physics*, 218(18), 1600562. DOI 10.1002/macp.201600562.
8. Prabunathan, P., Elumalai, P., Dinesh Kumar, G., Manoj, M., Hariharan, A. et al. (2020). Antiwetting and low-surface-energy behavior of cardanol-based polybenzoxazine-coated cotton fabrics for oil-water separation. *Journal of Coatings Technology and Research*, 17(6), 1455–1469. DOI 10.1007/s11998-020-00365-w.
9. Shen, X., Dai, J., Liu, Y., Liu, X., Zhu, J. (2017). Synthesis of high performance polybenzoxazine networks from bio-based furfurylamine: Furan vs. benzene ring. *Polymer*, 122(6), 258–269. DOI 10.1016/j.polymer.2017.06.075.
10. Wang, H., Zhao, P., Ling, H., Ran, Q., Gu, Y. (2013). The effect of curing cycles on curing reactions and properties of a ternary system based on benzoxazine, epoxy resin, and imidazole. *Journal of Applied Polymer Science*, 127(3), 2169–2175. DOI 10.1002/app.37778.

11. Zhang, K., Han, L., Froirniewicz, P., Ishida, H. (2018). Synthesis, polymerization kinetics and thermal properties of para-methylol functional benzoxazine. *Reactive and Functional Polymers*, 129(A), 23–28. DOI 10.1016/j.reactfunctpolym.2017.06.017.
12. Agag, T., Takeichi, T. (2001). Novel benzoxazine monomers containing p-phenyl propargyl ether: Polymerization of monomers and properties of polybenzoxazines. *Macromolecules*, 34(21), 7257–7263. DOI 10.1021/ma0107915.
13. Brunovska, Z., Ishida, H. (1999). Thermal study on the copolymers of phthalonitrile and phenylnitrile-functional benzoxazines. *Journal of Applied Polymer Science*, 73(14), 2937–2949. DOI 10.1002/(SICI)1097-4628(19990929)73:14<2937::AID-APP18>3.0.CO;2-E.
14. Chernykh, A., Agag, T., Ishida, H. (2009). Novel benzoxazine monomer containing diacetylene linkage: An approach to benzoxazine thermosets with low polymerization temperature without added initiators or catalysts. *Polymer*, 50(14), 3153–3157. DOI 10.1016/j.polymer.2009.04.061.
15. Feng, Z., Zeng, M., Meng, D., Chen, J., Zhu, W. et al. (2020). A novel bio-based benzoxazine resin with outstanding thermal and superhigh-frequency dielectric properties. *Journal of Materials Science: Materials in Electronics*, 31(5), 4364–4376. DOI 10.1007/s10854-020-02995-7.
16. Kudoh, R., Sudo, A., Endo, T. (2010). A highly reactive benzoxazine monomer, 1-(2-hydroxyethyl)-1,3-Benzoxazine: Activation of benzoxazine by neighboring group participation of hydroxyl group. *Macromolecules*, 43(3), 1185–1187. DOI 10.1021/ma902416h.
17. Liu, X., Zhang, R., Li, T., Zhu, P., Zhuang, Q. (2017). Novel fully biobased benzoxazines from rosin: Synthesis and properties. *ACS Sustainable Chemistry & Engineering*, 5(11), 10682–10692. DOI 10.1021/acssuschemeng.7b02650.
18. Niyomsin, S., Hirai, T., Takahara, A., Chirachanchai, S. (2019). Incorporation of benzoxazine pendants in polymer chains: A simple approach to add-up multi-responsive functions. *Macromolecular Chemistry and Physics*, 220(5), 1800526. DOI 10.1002/macp.201800526.
19. Wang, X., Zhou, S., Guo, W. W., Wang, P. L., Xing, W. et al. (2017). Renewable cardanol-based phosphate as a flame retardant toughening agent for epoxy resins. *ACS Sustainable Chemistry & Engineering*, 5(4), 3409–3416. DOI 10.1021/acssuschemeng.7b00062.
20. Xu, Y., Ran, Q., Li, C., Zhu, R., Gu, Y. (2015). Study on the catalytic prepolymerization of an acetylene-functional benzoxazine and the thermal degradation of its cured product. *RSC Advances*, 5(100), 82429–82437. DOI 10.1039/C5RA13862K.
21. Zhang, K., Liu, Y., Ishida, H. (2019). Polymerization of an AB-type benzoxazine monomer toward different polybenzoxazine networks: When Diels-Alder reaction meets benzoxazine chemistry in a single-component resin. *Macromolecules*, 52(19), 7386–7395. DOI 10.1021/acs.macromol.9b01581.
22. Zhang, S., Ran, Q., Fu, Q., Gu, Y. (2019). Carbonized polybenzoxazine for electromagnetic interference shielding. *Materials Chemistry and Physics*, 236, 121806. DOI 10.1016/j.matchemphys.2019.121806.
23. Zhang, Y., Liu, X., Zhan, G., Zhuang, Q., Zhang, R. et al. (2019). Study on the synergistic anticorrosion property of a fully bio-based polybenzoxazine copolymer resin. *European Polymer Journal*, 119(4), 477–486. DOI 10.1016/j.eurpolymj.2019.07.020.
24. Zhou, C., Tao, M., Liu, J., Xin, Z. (2019). Thermal curing behavior of benzoxazine functional polysilsesquioxane nanospheres. *Thermochimica Acta*, 678, 178295. DOI 10.1016/j.tca.2019.05.010.
25. Sha, X. L., Yuan, L., Liang, G., Gu, A. (2021). Heat-resistant and robust biobased benzoxazine resins developed with a green synthesis strategy. *Polymer Chemistry*, 12(3), 432–438. DOI 10.1039/D0PY01529F.
26. Ohashi, S., Rachita, E., Baxley, S., Zhou, J., Erlichman, A. et al. (2021). The first observation on polymerization of 1,3-benzoxazines: synthesis of mono- and bis-thiazine monomers and thermal properties of their polymers. *Polymer Chemistry*, 12(3), 379–388. DOI 10.1039/d0py01521k.
27. Kim, H. J., Brunovska, Z., Ishida, H. (1999). Molecular characterization of the polymerization of acetylene-functional benzoxazine resins. *Polymer*, 40(7), 1815–1822. DOI 10.1016/S0032-3861(98)00393-0.
28. Li, Y., Chen, D., Liu, X., Zhou, Y., Zhuang, Q. et al. (2014). Preparation of the PBOPy/PPy/Fe<sub>3</sub>O<sub>4</sub> composites with high microwave absorption performance and thermal stability. *Composites Science and Technology*, 100, 212–219. DOI 10.1016/j.compscitech.2014.06.013.

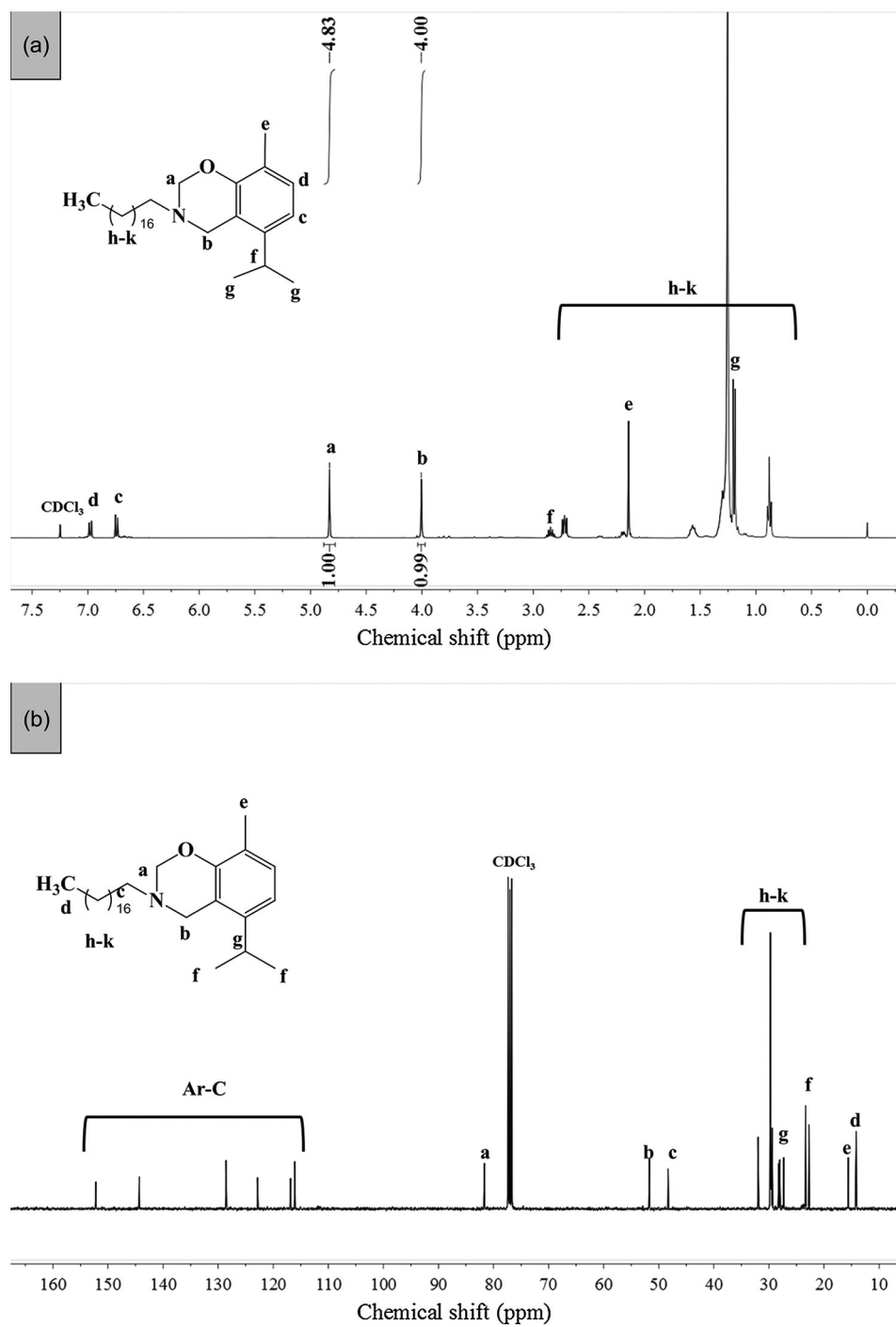


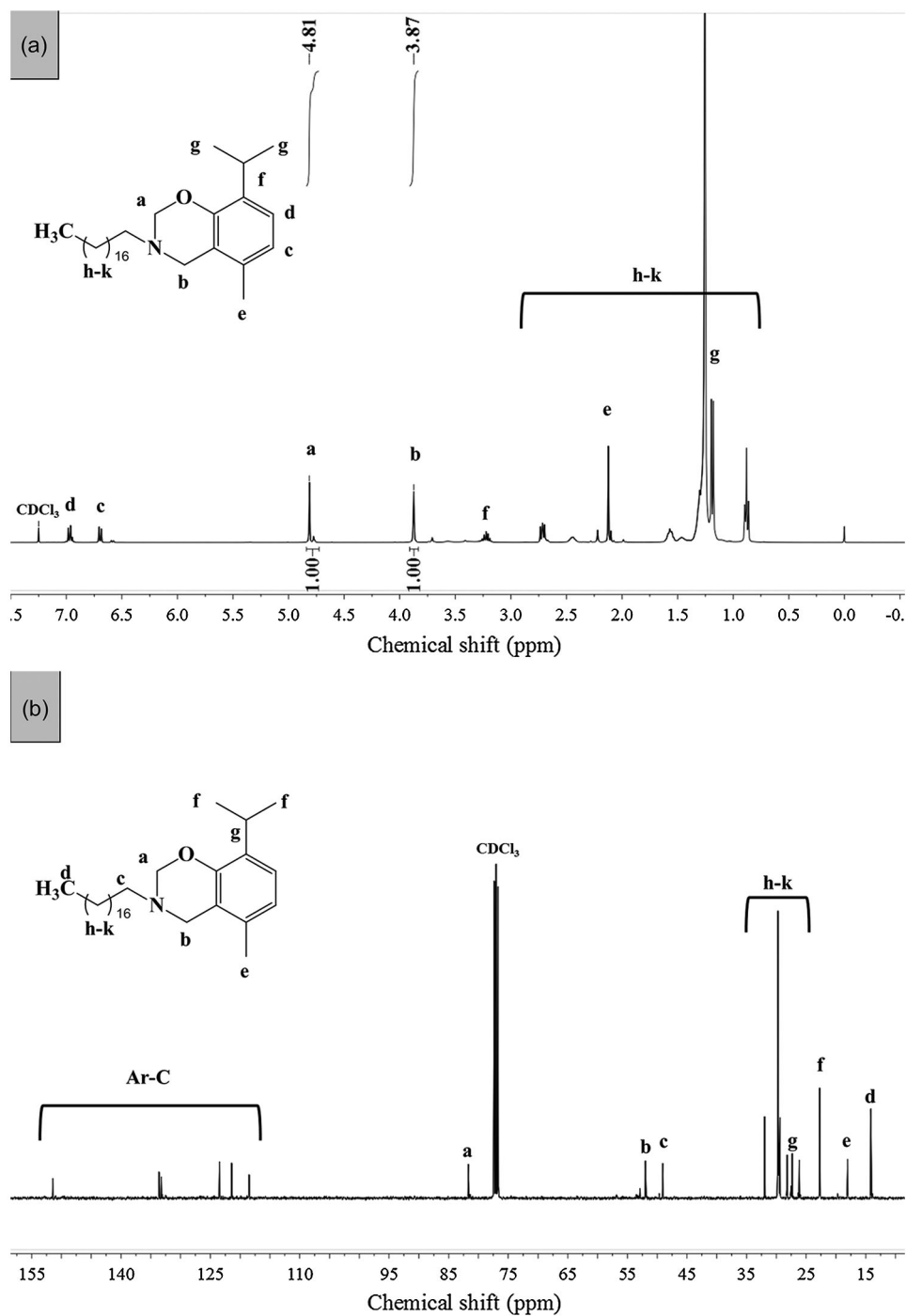
29. Zeng, K., Huang, J., Ren, J., Ran, Q. (2019). Curing reaction of Benzoxazine under high pressure and the effect on thermal resistance of Polybenzoxazine. *Macromolecular Chemistry and Physics*, 220(1), 1800340. DOI 10.1002/macp.201800340.
30. Zhang, K., Cai, R., Zhuang, Q., Liu, X., Yang, G. et al. (2014). High performance crosslinked system based on reaction of Benzoxazine with Benzoxazole. *Journal of Polymer Science Part A: Polymer Chemistry*, 52(11), 1514–1518. DOI 10.1002/pola.27153.
31. Zhang, K., Liu, J., Ohashi, S., Liu, X., Han, Z. et al. (2015). Synthesis of high thermal stability Polybenzoxazoles via Ortho-Imide-Functional Benzoxazine Monomers. *Journal of Polymer Science Part A: Polymer Chemistry*, 53(11), 1330–1338. DOI 10.1002/pola.27565.
32. Zhang, K., Zhuang, Q., Liu, X., Yang, G., Cai, R. et al. (2013). A new benzoxazine containing benzoxazole-functionalized polyhedral oligomeric silsesquioxane and the corresponding polybenzoxazine nanocomposites. *Macromolecules*, 46(7), 2696–2704. DOI 10.1021/ma400243t.
33. Zhang, K., Zhuang, Q., Zhou, Y., Liu, X., Yang, G. et al. (2012). Preparation and properties of novel low dielectric constant benzoxazole-based polybenzoxazine. *Journal of Polymer Science Part A: Polymer Chemistry*, 50(24), 5115–5123. DOI 10.1002/pola.26344.
34. Amarnath, N., Appavoo, D., Lochab, B. (2017). Eco-friendly halogen-free flame retardant cardanol polyphosphazene polybenzoxazine networks. *ACS Sustainable Chemistry & Engineering*, 6(1), 389–402. DOI 10.1021/acssuschemeng.7b02657.
35. Gao, S., Liu, Y., Feng, S., Lu, Z. (2017). Synthesis of Borosiloxane/Polybenzoxazine hybrids as highly efficient and environmentally friendly flame retardant materials. *Journal of Polymer Science Part A: Polymer Chemistry*, 55(14), 2390–2396. DOI 10.1002/pola.28628.
36. Liu, X., Li, Z., Zhan, G., Wu, Y., Zhuang, Q. (2019). Bio-based benzoxazines based on sesamol: Synthesis and properties. *Journal of Applied Polymer Science*, 136(48), 48255. DOI 10.1002/app.48255.
37. Mohamed, M. G., Kuo, S. W. (2020). Crown ether-functionalized polybenzoxazine for metal ion adsorption. *Macromolecules*, 53(7), 2420–2429. DOI 10.1021/acs.macromol.9b02519.
38. Zhang, K., Zhuang, Q., Liu, X., Cai, R., Yang, G. et al. (2013). Synthesis and copolymerization of benzoxazines with low-dielectric constants and high thermal stability. *RSC Advances*, 3(15), 5261–5270. DOI 10.1039/c3ra22471f.
39. Hong, L., Ju, S., Liu, X., Zhuang, Q., Zhan, G. et al. (2019). Highly selective CO<sub>2</sub> uptake in novel fishnet-like polybenzoxazine-based porous carbon. *Energy & Fuels*, 33(11), 11454–11464. DOI 10.1021/acs.energyfuels.9b02631.
40. Monisha, Shukla, S., Lochab, B. (2017). Nanoparticles as curing and adhesive aid for biobased and petrobased polybenzoxazines. *Green Materials*, 5(2), 94–102. DOI 10.1680/jgrma.17.00004.
41. Zhou, C., Lin, J., Lu, X., Xin, Z. (2016). Enhanced corrosion resistance of polybenzoxazine coatings by epoxy incorporation. *RSC Advances*, 6(34), 28428–28434. DOI 10.1039/C6RA02215D.
42. Mohamed, M. G., Kuo, S. W. (2019). Functional silica and carbon nanocomposites based on polybenzoxazines. *Macromolecular Chemistry and Physics*, 220(1), 1800306. DOI 10.1002/macp.201800306.
43. Sini, N. K., Endo, T. (2016). Toward elucidating the role of number of oxazine rings and intermediates in the benzoxazine backbone on their thermal characteristics. *Macromolecules*, 49(22), 8466–8478. DOI 10.1021/acs.macromol.6b01965.
44. Timur, M., Nur, Y., Sikar, H. (2019). Synthesis of Schiff base-containing benzoxazine derivatives. *Journal of Applied Polymer Science*, 136(35), 47908. DOI 10.1002/app.47908.
45. Zhang, S., Ran, Q., Fu, Q., Gu, Y. (2019). Controlled polymerization of 3,4-dihydro-2H-1,3-benzoxazine and its properties tailored by Lewis acids. *Reactive & Functional Polymers*, 139(11), 75–84. DOI 10.1016/j.reactfunctpolym.2019.03.016.
46. Sudo, A., Du, L. C., Hirayama, S., Endo, T. (2010). Substituent effects of N-Alkyl groups on thermally induced polymerization behavior of 1,3-benzoxazines. *Journal of Polymer Science Part A: Polymer Chemistry*, 48(13), 2777–2782. DOI 10.1002/pola.24026.

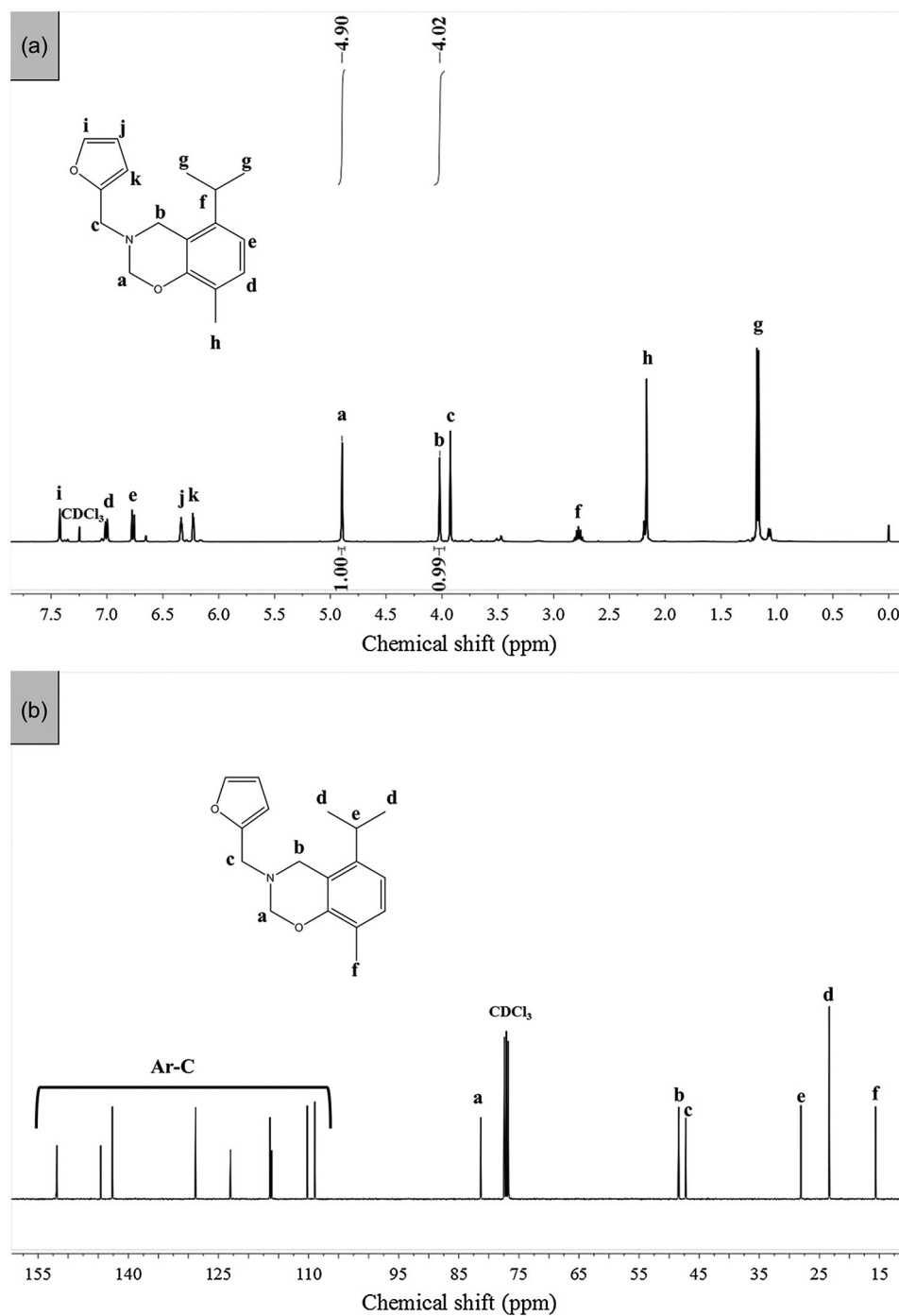
47. Martos, A., Soto, M., Schafer, H., Koschek, K., Marquet, J. et al. (2020). Highly crosslinked polybenzoxazines from monobenzoxazines: The effect of meta-substitution in the phenol ring. *Polymers*, 12(2), 254. DOI 10.3390/polym12020254.
48. Kolanadiyil, S. N., Minami, M., Endo, T. (2017). Synthesis and thermal properties of difunctional benzoxazines with attached oxazine ring at the para-, meta-, and ortho-position. *Macromolecules*, 50(9), 3476–3488. DOI 10.1021/acs.macromol.7b00487.
49. Lyu, Y., Rachita, E., Pogharian, N., Froimowicz, P., Ishida, H. (2020). Electronic effects of asymmetric and meta-alkoxy substituents on the polymerization behavior of bis-benzoxazines. *Polymer Chemistry*, 11(4), 800–809. DOI 10.1039/C9PY01641D.
50. Wang, X., Chen, F., Gu, Y. (2011). Influence of electronic effects from bridging groups on synthetic reaction and thermally activated polymerization of bisphenol-based benzoxazines. *Journal of Polymer Science Part A: Polymer Chemistry*, 49(6), 1443–1452. DOI 10.1002/pola.24566.
51. Andreu, R., Reina, I. A., Ronda, J. C. (2008). Studies on the thermal polymerization of substituted benzoxazine monomers: Electronic effects. *Journal of Polymer Science Part A: Polymer Chemistry*, 46(10), 3353–3366. DOI 10.1002/pola.22677.
52. Wazarkar, K., Sabnis, A. (2018). Effect of pendant functional groups on curing kinetics and final properties of cardanol-based benzoxazines. *Journal of Coatings Technology and Research*, 15(3), 555–569. DOI 10.1007/s11998-017-0020-9.
53. Martos, A., Sebastian, R. M., Marquet, J. (2018). Studies on the ring-opening polymerization of benzoxazines: Understanding the effect of the substituents. *European Polymer Journal*, 108, 20–27. DOI 10.1016/j.eurpolymj.2018.08.025.
54. Biru, E. I., Garea, S. A., Iovu, H. (2019). Developing polybenzoxazine composites based on various carbon structures. *Macromolecular Chemistry and Physics*, 220(3), 1800322. DOI 10.1002/macp.201800322.
55. Dai, J., Yang, S., Teng, N., Liu, Y., Liu, X. et al. (2018). Synthesis of eugenol-based silicon-containing benzoxazines and their applications as bio-based organic coatings. *Coatings*, 8(3), 88. DOI 10.3390/coatings8030088.
56. Monisha, M., Amarnath, N., Mukherjee, S., Lochab, B. (2019). Cardanol benzoxazines: A versatile monomer with advancing applications. *Macromolecular Chemistry and Physics*, 220(3), 1800470. DOI 10.1002/macp.201800470.
57. Peng, Y., Dai, J., Liu, Y., Cao, L., Zhu, J. et al. (2019). Bio-based polybenzoxazine modified melamine sponges for selective absorption of organic solvent in water. *Advanced Sustainable Systems*, 3(3), 1800126. DOI 10.1002/advs.201800126.
58. Bayram, K., Kiskan, B., Yagci, Y. (2021). Synthesis of thioamide containing polybenzoxazines by the Willgerodt-Kindler reaction. *Polymer Chemistry*, 12(4), 534–544. DOI 10.1039/D0PY01381A.
59. Chatterjee, M., Ishizaka, T., Kawanami, H. (2016). Reductive amination of furfural to furfurylamine using aqueous ammonia solution and molecular hydrogen: An environmentally friendly approach. *Green Chemistry*, 18(2), 487–496. DOI 10.1039/C5GC01352F.
60. Chandra, D., Inoue, Y., Sasase, M., Kitano, M., Bhaumik, A. et al. (2018). A high performance catalyst of shape-specific ruthenium nanoparticles for production of primary amines by reductive amination of carbonyl compounds. *Chemical Science*, 9(27), 5949–5956. DOI 10.1039/C8SC01197D.
61. Li, X., Jia, P., Wang, T. (2016). Furfural: A promising platform compound for sustainable production of C4 and C5 Chemicals. *ACS Catalysis*, 6(11), 7621–7640. DOI 10.1021/acscatal.6b01838.
62. Lange, J. P., van der Heide, E., van Buijtenen, J., Price, R. (2012). Furfural: A promising platform for lignocellulosic biofuels. *ChemSusChem*, 5(1), 150–166. DOI 10.1002/cssc.201100648.
63. Wang, C., Sun, J., Liu, X., Sudo, A., Endo, T. (2012). Synthesis and copolymerization of fully bio-based benzoxazines from guaiacol, furfurylamine and stearylamine. *Green Chemistry*, 14(10), 2799. DOI 10.1039/c2gc35796h.
64. Gozzi, C., Convard, A., Husset, M. (2009). Heterogeneous acid-catalysed isomerization of carvone to carvacrol. *Reaction Kinetics and Catalysis Letters*, 97(2), 301–306. DOI 10.1007/s11144-009-0030-4.

65. Coccimiglio, J., Alipour, M., Jiang, Z. H., Gottardo, C., Suntres, Z. (2016). Antioxidant, antibacterial, and cytotoxic activities of the ethanolic *origanum vulgare* extract and its major constituents. *Oxidative Medicine and Cellular Longevity*, 2016(2), 1–8. DOI 10.1155/2016/1404505.
66. Kfoury, M., Landy, D., Ruellan, S., Auezova, L., Greige-Gerges, H. et al. (2016). Determination of formation constants and structural characterization of cyclodextrin inclusion complexes with two phenolic isomers: Carvacrol and thymol. *Beilstein Journal of Organic Chemistry*, 12, 29–42. DOI 10.3762/bjoc.12.5.
67. Llana-Ruiz-Cabello, M., Pichardo, S., Maisanaba, S., Puerto, M., Prieto, A. I. et al. (2015). In vitro toxicological evaluation of essential oils and their main compounds used in active food packaging: A review. *Food and Chemical Toxicology*, 81(S1), 9–27. DOI 10.1016/j.fct.2015.03.030.
68. Promdee, K., Vitidsant, T. (2013). Bio-oil synthesis by pyrolysis of cogongrass (*Imperata Cylindrica*). *Chemistry and Technology of Fuels and Oils*, 49(4), 287–292. DOI 10.1007/s10553-013-0443-7.
69. Hitschler, J., Boles, E. (2020). Improving 3-methylphenol (m-cresol) production in yeast via *in vivo* glycosylation or methylation. *FEMS Yeast Research*, 20(8), 1–12. DOI 10.1093/femsyr/foaa063.
70. Jubsilp, C., Damrongsakkul, S., Takeichi, T., Rimdusit, S. (2006). Curing kinetics of arylamine-based polyfunctional benzoxazine resins by dynamic differential scanning calorimetry. *Thermochimica Acta*, 447(2), 131–140. DOI 10.1016/j.tca.2006.05.008.
71. Andronescu, C., Garea, S. A., Deleanu, C., Iovu, H. (2012). Characterization and curing kinetics of new benzoxazine monomer based on aromatic diamines. *Thermochimica Acta*, 530, 42–51. DOI 10.1016/j.tca.2011.11.035.

## Appendix

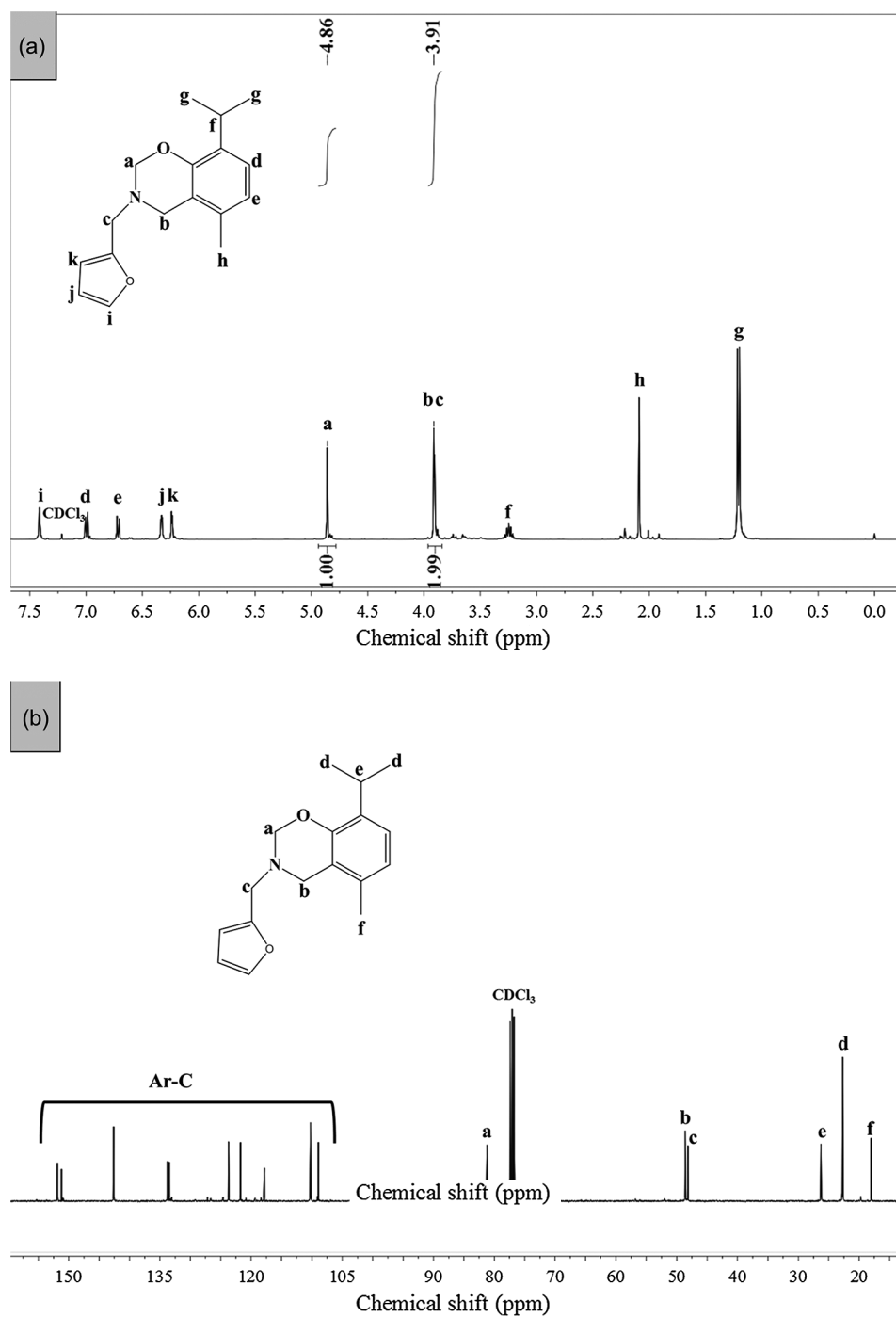
**Figure S1:** (a) <sup>1</sup>H-NMR, (b) <sup>13</sup>C-NMR spectrum of  $m_1$

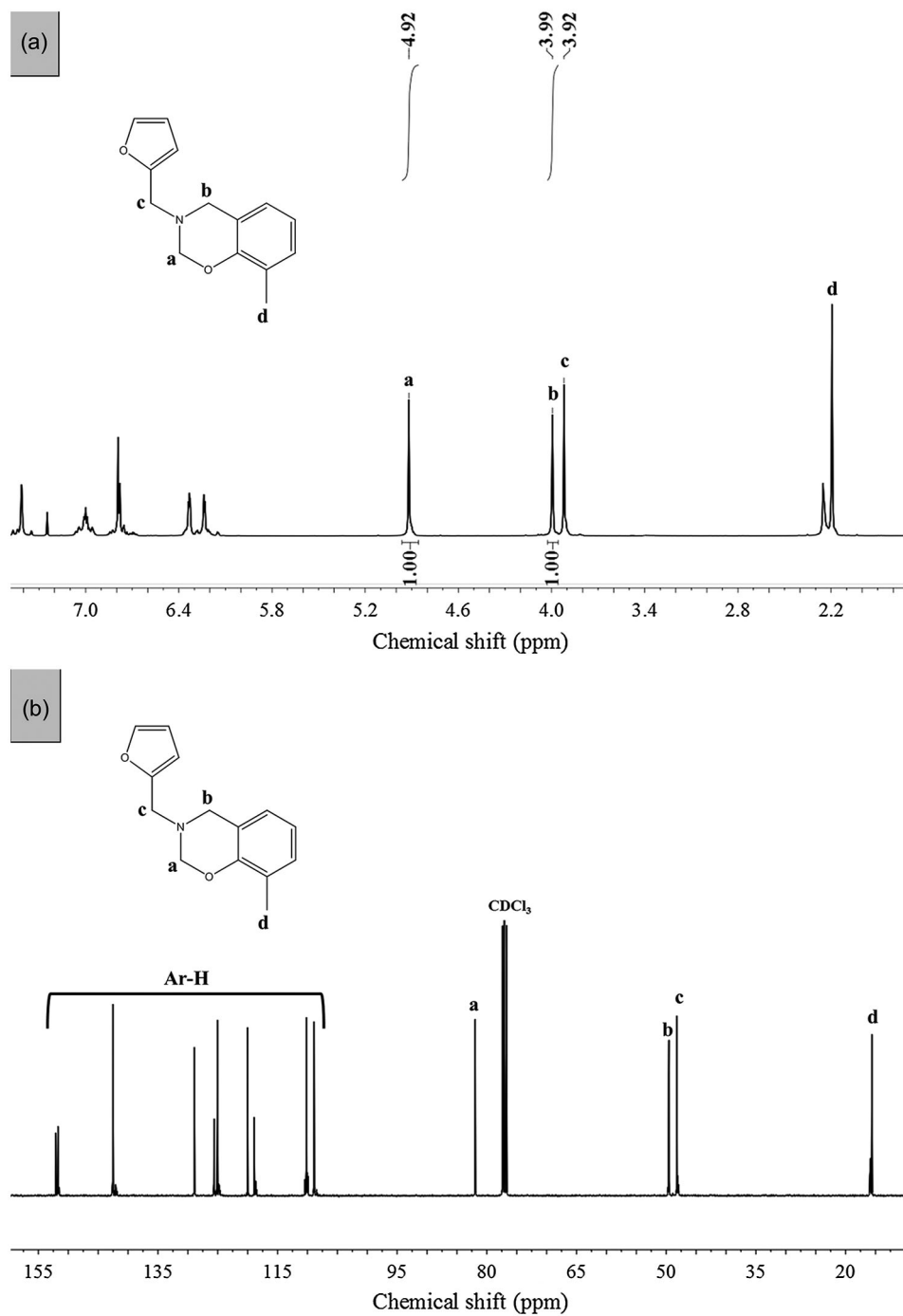
**Figure S2:** (a)  $^1H$ -NMR, (b)  $^{13}C$ -NMR spectrum of  $m_2$



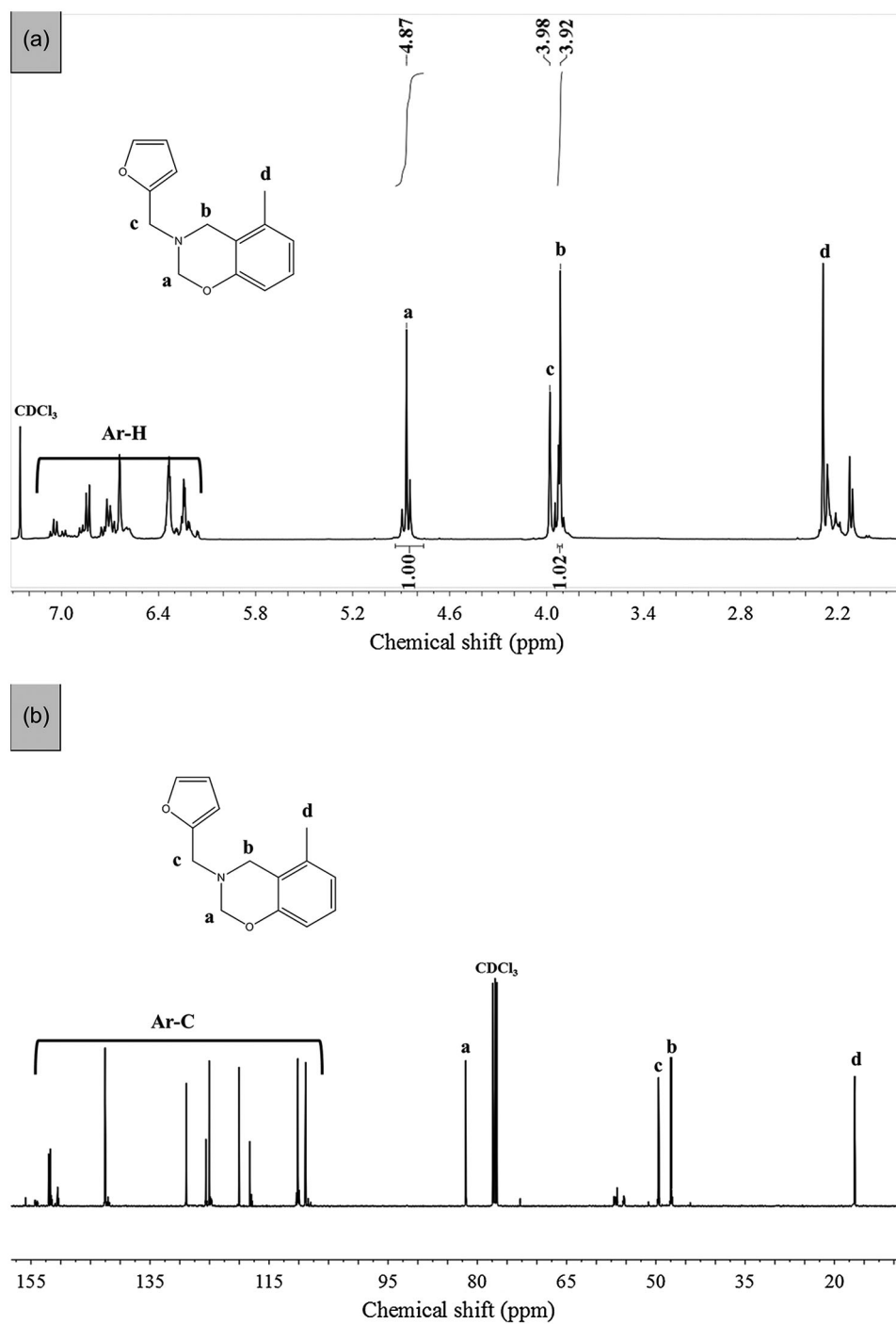
**Figure S3:** (a)  $^1\text{H}$ -NMR, (b)  $^{13}\text{C}$ -NMR spectrum of  $m_3$

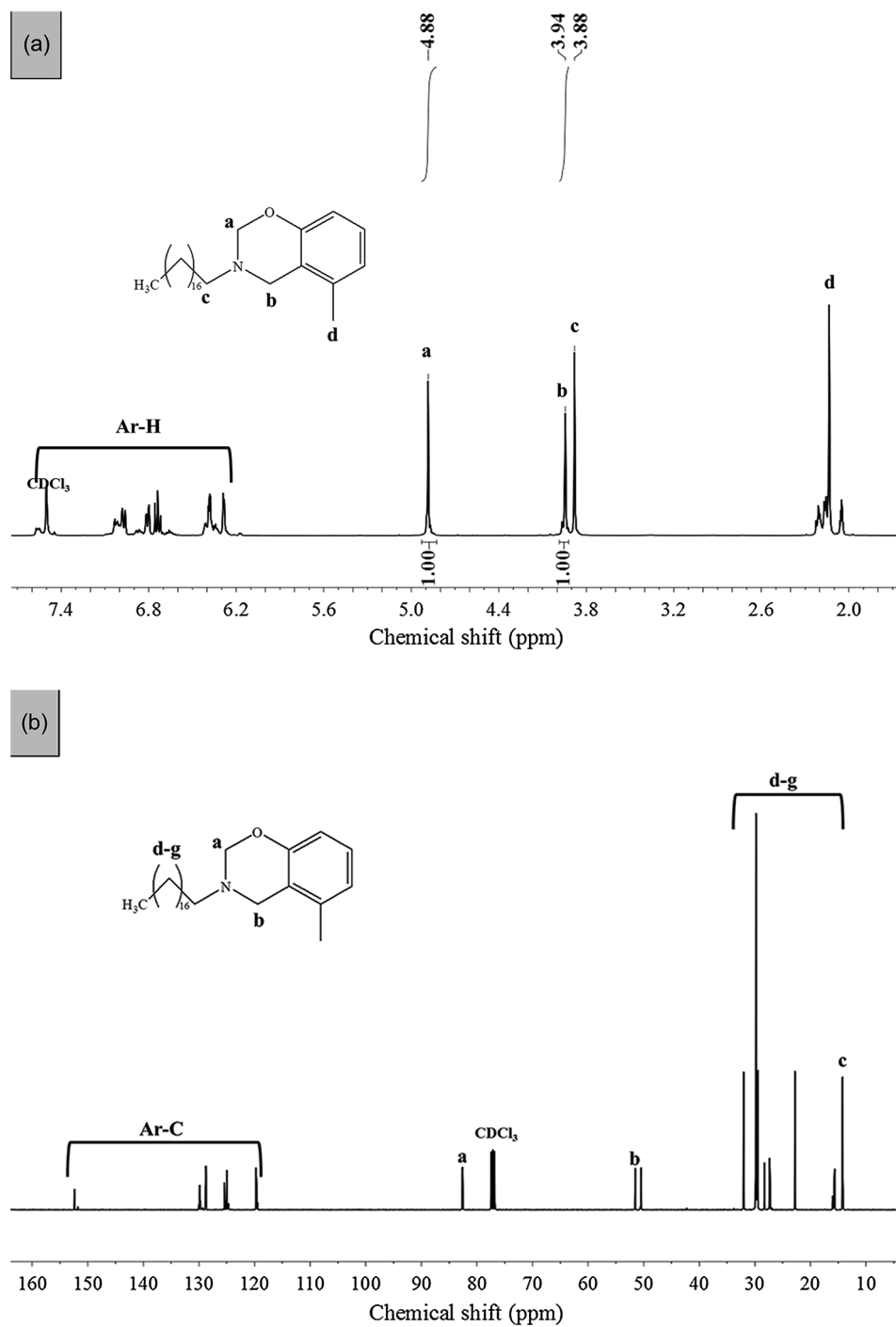




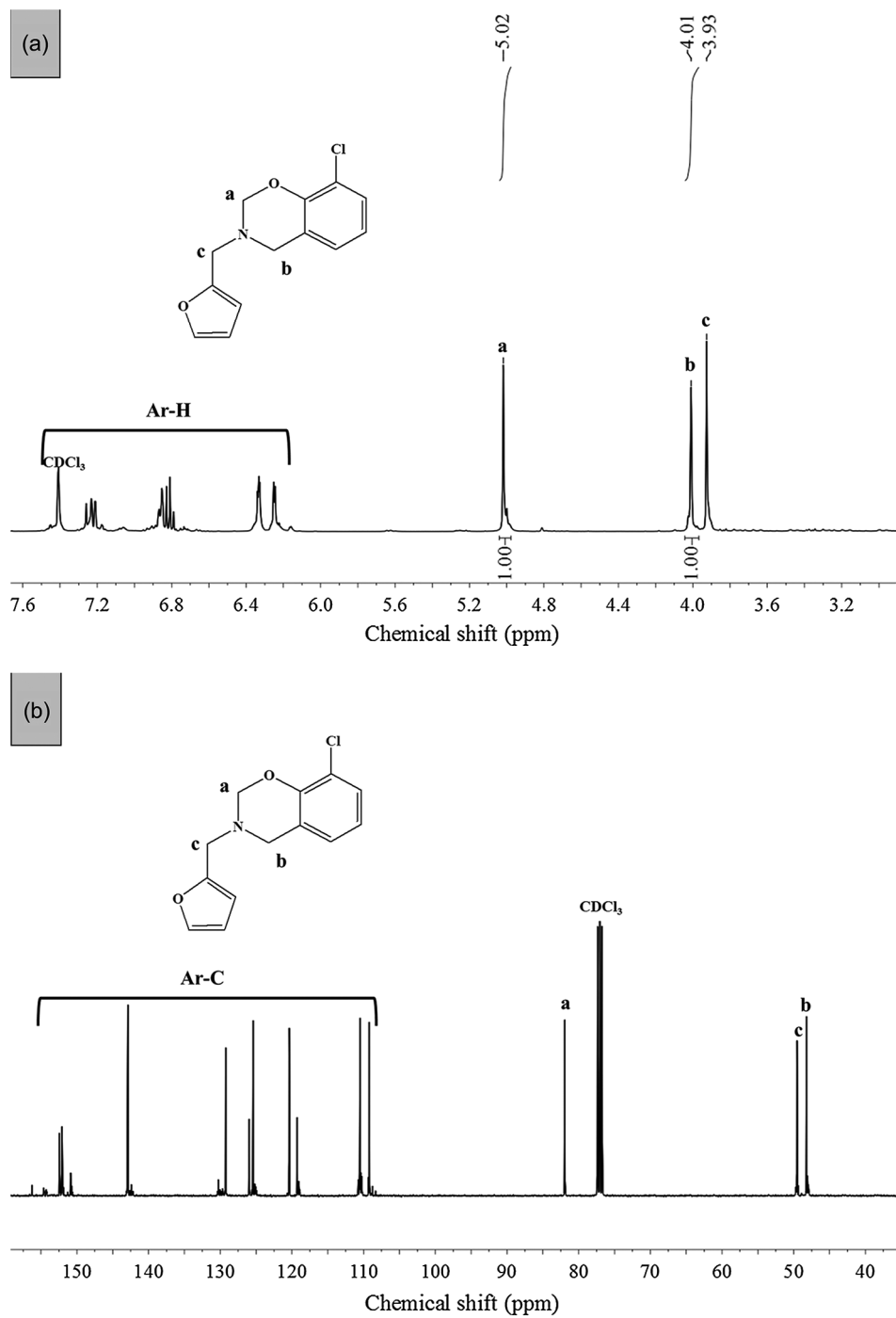


**Figure S5:** (a)  $^1\text{H}$ -NMR, (b)  $^{13}\text{C}$ -NMR spectrum of  $m_5$

**Figure S6:** (a) <sup>1</sup>H-NMR, (b) <sup>13</sup>C-NMR spectrum of **m<sub>6</sub>**



**Figure S7:** (a) <sup>1</sup>H-NMR, (b) <sup>13</sup>C-NMR spectrum of **m7**

**Figure S8:** (a) <sup>1</sup>H-NMR, (b) <sup>13</sup>C-NMR spectrum of **m8**